

Performance evaluation and hysteretic modeling of low rise reinforced concrete shear walls

T. Nagender^{1a}, Y.M. Parulekar^{*1} and G. Appa Rao²

¹Reactor Safety Division, Bhabha Atomic Research Centre, Trombay, Mumbai-400085, India

²Department of Civil Engineering, Indian Institute of Technology Madras, Chennai, Tamil Nadu-600036, India

(Received May 3, 2018, Revised October 26, 2018, Accepted December 1, 2018)

Abstract. Reinforced Concrete (RC) shear walls are widely used in Nuclear power plants as effective lateral force resisting elements of the structure and these may experience nonlinear behavior for higher earthquake demand. Short shear walls of aspect ratio less than 1.5 generally experience combined shear flexure interaction. This paper presents the results of the displacement-controlled experiments performed on six RC short shear walls with varying aspect ratios (1, 1.25 and 1.5) for monotonic and reversed quasi-static cyclic loading. Simulation of the shear walls is then carried out by Finite element modeling and also by macro modeling considering the coupled shear and flexure behaviour. The shear response is estimated by softened truss theory using the concrete model given by Vecchio and Collins (1994) with a modification in softening part of the model and flexure response is estimated using moment curvature relationship. The accuracy of modeling is validated by comparing the simulated response with experimental one. Moreover, based on the experimental work a multi-linear hysteretic model is proposed for short shear walls. Finally ultimate load, drift, ductility, stiffness reduction and failure pattern of the shear walls are studied in details and hysteretic energy dissipation along with damage index are evaluated.

Keywords: short shear walls; hysteretic model; cyclic; ductility; experiments

1. Introduction

Reinforced concrete shear walls act as major earthquake resisting members in design of buildings and these are the main structural elements of Nuclear Power Plants (NPPs). Failure of these shear walls is quite complex and depend on parameters like aspect ratio, axial load ratio, presence of boundary elements and reinforcement percentage. Hence, realistic evaluation of performances of shear walls subjected to earthquake is the subject of research. The methodology needs to be developed and validated with experiments for different aspect ratios of shear walls. Therefore, scientific research in this area is very intensive and has resulted in many experimental programme and analytical model development in the past years. Due to the parameter variability of shear walls and complex behaviour, each experimental or numerical research is but a contribution to the knowledge database. Models for evaluation of hysteretic characteristics of short shear walls have shown limited progress.

Low-rise walls are different from both slender and squat walls due to the fact that these walls are not controlled entirely by either shear or flexure, but rather a combination of the two. The various modes of failure of shear walls include flexure, shear evident with diagonal crushing or tension cracking and sliding shear caused by interface shear

transfer failures at horizontal cracks. All these modes of failure are emphasized by tests carried out by various researchers. Earlier experiments have been carried out on low rise shear walls (Lopes *et al.* 2001). He tested four small-scale reinforced concrete walls each with aspect ratio 1.9 and with different amount of shear reinforcement under cyclic loading. All the shear walls failed in shear either by diagonal tension or diagonal crushing. The yield strength of the stirrups was exceeded in all walls which were failed in shear by diagonal tension and in the wall which were failed by concrete crushing, some stirrups did not yield. Salonikios *et al.* (1999) conducted tests on shear walls with aspect ratios of 1.0 and 1.5. The wall specimens were reinforced against shear, either conventionally (orthogonal grids of web reinforcement) or with cross-inclined bars. The specimens were tested as cantilevers and those having diagonal reinforcement failed in a predominantly flexural mode, characterized by concrete crushing and reinforcement buckling. Griefenhagen and Lestuzzi (2005) tested four lightly reinforced shear walls with aspect ratio 0.69 under cyclic loading. They observed substantially different crack patterns for shear related failure modes such as sliding, diagonal compression, and diagonal tension in all specimens due to variation of the concrete compressive strength and the axial force. Recently, in 2017, experimental investigation was carried out by Christidis and Trezos (2017) to assess and strengthen existing non-conforming reinforced concrete midrise walls of aspect ratio 2 designed according to older seismic codes that do not meet the modern seismic provisions. They concluded that low ratios of shear reinforcement do not seem to affect either the bearing or the top deformation capacity of the walls

*Corresponding author, Ph.D.

E-mail: ymparulekar@gmail.com

^aScientific Officer

significantly. Habibi *et al.* (2018), recently compared the energy dissipation capacities and ductility of shear walls made of alkali silica reactive (ASR) concrete with that of shear walls made with normal concrete. They concluded that both the ductility and energy dissipation capabilities of shear walls decreased by 25-30% due to ASR.

Modelling of RC walls involves several challenges in representing the combined effects of moment, shear and axial forces, in addition to bar slip, buckling, damping and boundary conditions. The models are classified as micro-models such as finite element models and fibre models and macro-models such as strut or beam model. Fibre model was used by Kotronis *et al.* (2005) to simulate the behaviour of RC shear walls under dynamic excitation. They simulated shake table experimental campaigns of CAMUS I and III using Bernoulli multilayered beam elements and advanced constitutive laws based on damage mechanics and plasticity. The proposed strategy could reproduce the global behaviour of the specimens but its major drawback was that it could not capture localized, discrete phenomena like excessive plastic deformations and significant cracks. In 2016, Jeong and Jang predicted inelastic response of RC shear walls using fiber and spring elements. The fiber elements and the spring reflect flexural and shear behaviors of the shear wall, respectively. Recently, a rational analysis procedure was given by Feng *et al.* (2018) for modeling cyclic behavior of reinforced concrete shear walls based on softened damage-plasticity model considering compression-softening effect. Parulekar *et al.* in 2014 carried out simulation of RC stiff squat shear wall tested in test program called TESSH at JRC, Italy using Finite element modelling and analysis. Three-dimensional and two-dimensional FE models predicted the load displacement characteristics as well as crack patterns obtained by tests with sufficient accuracy. However, these approaches were computationally cumbersome and hence macro-modelling approach which guaranteed simplicity was used by researchers. The cyclic testing of the same full-scale low aspect ratio reinforced concrete wall in a principally uniform shear state was described by Beko *et al.* in 2015 and a nonlinear mathematical model was described which is capable of simulating the hysteresis of the tested shear walls. However this model was based on test results of one shear wall configuration only. Simplified approach to accurately predict the load deformation behaviour of shear walls was first proposed by Vecchio and Collins in 1986 using modified compression field theory. Later, macro-models such as three vertical line elements (TVLE) connected to each other by rigid bars at the top and the bottom wall was developed into multiple vertical line element by Vulcano *et al.* (1988). However, in these models the deformation compatibility between the wall and the boundary element was still not enforced and the flexure and shear responses were not coupled. Softened-Strut-and-Tie truss model was then used by Yu and Hwang (2005) to predict the shear capacity of RC squat walls. Later, Wallace *et al.* (2008) modified the model proposed by Yu and Hwang (2005) considering the coupled response to improve the efficiency of the model in predicting the response of RC shear walls. It is worth noting that, although such models were able to predict the capacity of RC elements, they could not capture the cyclic or the hysteretic behaviour of these

elements. Lot of hysteretic models have been developed in past for RC shear walls like Takeda model by Takeda *et al.* (1970), modified Takeda model by Otani (1974), Q model by Saiidi and Sozen (1981), gamma model by Lestuzzi *et al.* (2003). On the basis of experimental testing hysteretic models were suggested by Brun *et al.* (2003) considering stiffness degradation and Thomson *et al.* (2009) considering pinching effect. Later Brun *et al.* (2011) carried out pseudo-dynamic tests on low-shear walls and proposed a simplified model based on the structural frequency drift. In 2016, Parulekar *et al.* tested midrise shear walls and suggested simplified hysteretic model for dynamic behaviour of these walls. Saritas *et al.* (2013) has proposed a 3D plastic damage model to describe the hysteretic behaviour of concrete. The proposed model was able to capture the overall load-deformation response of RC structural walls of varying aspect ratios. However this 3D model was complex.

It was observed from work carried out by the researchers that aspect ratios, axial load ratio and percentage reinforcement play a significant role in the mode of failure, the ultimate load, drift and hysteretic characteristics of the shear walls. It is therefore required to systematically evolve a simplified methodology and suggest a multi-linear hysteretic model for short shear walls which is based on particular range of axial load ratio and reinforcement ratio. The hysteretic models suggested by researchers till date for short shear walls are not applicable for various axial load ratios and reinforcement ratios. This is so because the hysteretic characteristics such as stiffness degradation and pinching are path dependent and differ for same shear wall with varying axial loads and varying reinforcement ratio. Hence the novelty of the present work is that a multi-linear hysteretic model is given for short shear walls by carrying out experimental studies on six numbers of lightly reinforced shear walls (0.45% reinforcement in vertical direction and 0.36% to 0.4% in horizontal direction) with aspect ratios ranging from 1 to 1.5 and an axial load ratio of 1%. Moreover, experimental responses of lightly reinforced shear walls from literature of similar aspect ratio and axial load ratio are also used for validation of the model. From the experiments performed in the present study, ultimate load, drift, ductility, stiffness reduction and failure pattern of the walls are studied. Macro-modelling approach is adopted considering the coupled shear and flexure behaviour for shear walls to obtain backbone curve for the shear walls. The shear response is estimated using softened truss theory and using the concrete model given by Vecchio and Collins (1994) with a modification in softening part of the model and flexure response is estimated using moment curvature relationship. Finite element analysis is also performed using appropriate constitutive model which is formulated on the basis of nonlinearity of concrete and reinforcement. Comparison of analysis and test results is presented clearly.

2. Experimental program

Six RC short shear walls with boundary elements were cast and tested under monotonic and cyclic loading conditions.

Table 1 Specifications of the Test specimens

Specimen and Dimensions	Aspect Ratio	Concrete Cube Compressive strength (MPa)		Steel Diameter (mm)	Yield stress (MPa)	Ultimate stress (MPa)	% steel Vertical	% steel Horizontal
		7 days	28 days					
SW1 (Mono) 1.5 m×1 m×0.15 m	1.5	14.22	22.22	8 16	437.67 423.56	586.88 563.33	0.45	0.36
SW2 (Cyc) 1.5 m×1 m×0.15 m	1.5	15.26	23.48	8 16	439.52 440.56	584.56 585.46	0.45	0.36
SW3 (Mono) 1.25 m×1 m×0.15 m	1.25	15.59	23.63	8 16	429.85 426.35	567.41 569.17	0.45	0.38
SW4 (Cyc) 1.25 m×1 m×0.15 m	1.25	16.16	24.12	8 16	431.26 435.23	560.22 574.53	0.45	0.38
SW5 (Mono) 1 m×1 m×0.15 m	1	16.64	26.42	8 16	428.53 432.56	569.94 570.25	0.45	0.4
SW6 (Cyc) 1 m×1 m×0.15 m	1	18.82	29.85	8 16	421.35 435.23	556.182 570.15	0.45	0.4

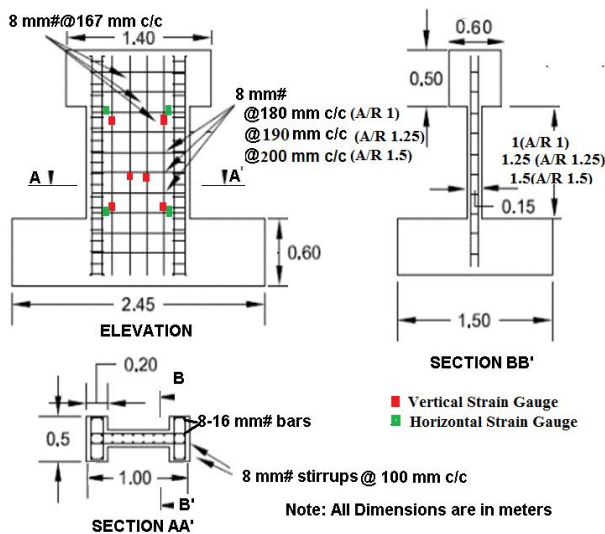


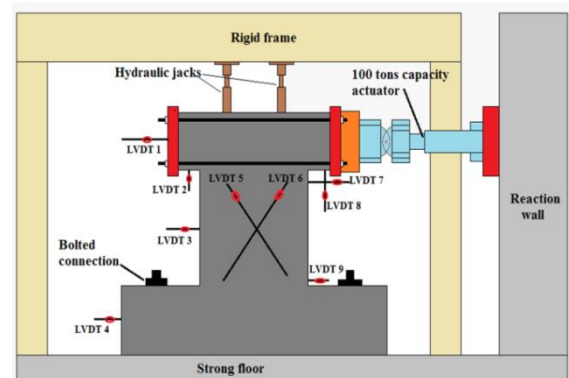
Fig. 1 Shear walls: Reinforcement details and location of Strain gauges

2.1 Wall specifications

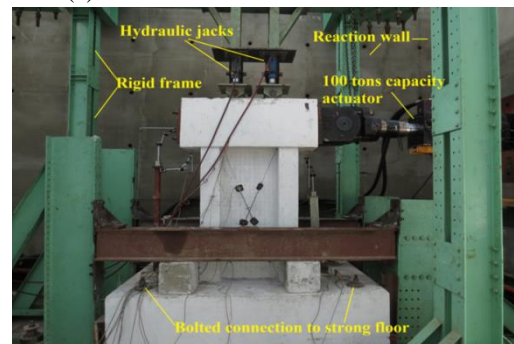
The sectional dimensions and reinforcement details of the shear wall specimens are shown in Fig. 1. All the test specimens had a web thickness of 150 mm and width of 1000 mm. Heights of the specimens were different depending on aspect ratios and specifications of the tests specimens are given in Table 1. Each of the six specimens consisted of flanged wall connected to a heavily reinforced concrete base block which was anchored and locked to the strong floor in the laboratory. The schematic test setup and the actual test setup are shown in Fig. 2(a) and Fig. 2(b) respectively. A deep heavily reinforced concrete top block was also connected at the top of the wall for the lateral load application. In all the six specimens, reinforcement percentage in both horizontal and vertical directions is given in Table 1. In each of the boundary elements twelve steel bars of 16mm diameter were used as longitudinal bars and 8mm diameter bars were used as stirrups (Fig. 1).

2.2 Material properties

The shear walls were designed using concrete with cube



(a) Schematic and location of LVDTs



(b) Actual test setup

Fig. 2 Test setup of Shear walls

strength (f_{ck}) of 20 N/mm² and reinforcement steel with yield strength of 415 N/mm². Six cubes were cast for every concrete mix. Three cubes were tested at 7 days and the other three at 28 days of curing. The average compressive strength of the cubes tested at 28 days of each specimen listed in Table 1. Samples of the reinforcing steel used in wall specimens were collected and tested under direct tension to determine their yield and ultimate strengths. The results of the specimen tests on concrete cubes and reinforcement bars are summarized in Table 1

2.3 Instrumentation

Strains in the reinforcement bars were measured using electrical resistance strain gauges attached to the reinforcing

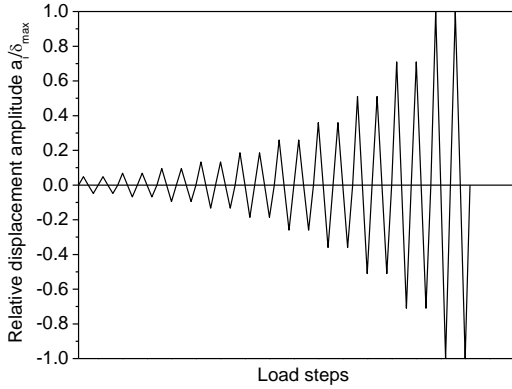


Fig. 3 Loading protocol

bars at 10 locations as shown in Fig. 1. Four numbers of strain gauges were attached to horizontal reinforcement and six numbers of strain gauges were attached to vertical reinforcement. The locations of the LVDTs placed on the shear wall at bottom and top are shown in Fig. 2(a). One face of each specimen was instrumented with LVDTs (LVDT1, LVDT 3, LVDT 7 and LVDT9) positioned horizontally. LVDT5 and LVDT6 are attached diagonally to monitor average shear strain distortions and rotations. LVDT4 is attached between the base block and a fixed location at support to ensure fixity of the base. The rotation of the bottom and top blocks was monitored using LVDT2 and LVDT 8 placed vertically at the edges.

2.4 Testing procedures

The 100 tons capacity actuator was used for applying lateral displacement on the specimens through the top block as shown in the test setup in Fig. 2(b). The lateral movement of the specimen base was arrested by fixing the bottom block of the specimen with the strong floor of lab

using bolts and two ‘A’ frames were provided at the ends of the specimen. The applied loads (reactions) were measured using the load cells. The top beam of the specimen was loaded vertically using the hydraulic jack with a total compression load of 6 tons which gives an axial load ratio ($N/A_g f_{ck}$) of 1%. Later, the monotonic loading was applied using actuator to the three specimens (SW1, SW3, and SW5) with different aspect ratios. The walls were loaded till failure i.e., till the reaction in the load cell dropped to 85% of the peak load. The remaining three wall specimens (SW2, SW4, and SW6) were subjected to the cyclic loads in order to simulate the loading sequence that might be expected to occur during an earthquake. The loading protocol for applying cyclic loading for the respective specimens was adopted as per FEMA-461. The amplitude, a_{i+1} of the step $i+1$ is 1.4 times the amplitude (a_i) of i th step. The loading protocol is shown in Fig. 3.

Horizontal load was applied at a quasi-static rate in displacement-controlled cycles which corresponded to three major states, namely cracking state, yielding state and ultimate state. The rate of loading began at 0.05 mm/s and later it was increased till 0.1 mm/s. First two cycles were applied such that the wall remains in pre-cracking stage in the complete cycles and hence the lateral displacement amplitude of 0.3 mm peak was given in first two cycles. Later the amplitudes of subsequent cycles were given as 1.4 times that of the previous cycle. Every excursion in the inelastic range causes cumulative damage in the structural elements. For each amplitude, two complete cycles were given and repetition in excursions were made because it is generally observed that there is a drop in the peak load after the first cycle and then stabilization is achieved. Lateral load excursions were applied till the significant drop of 15% in the peak load was achieved and this was marked as the failure of walls

2.5 Experimental results

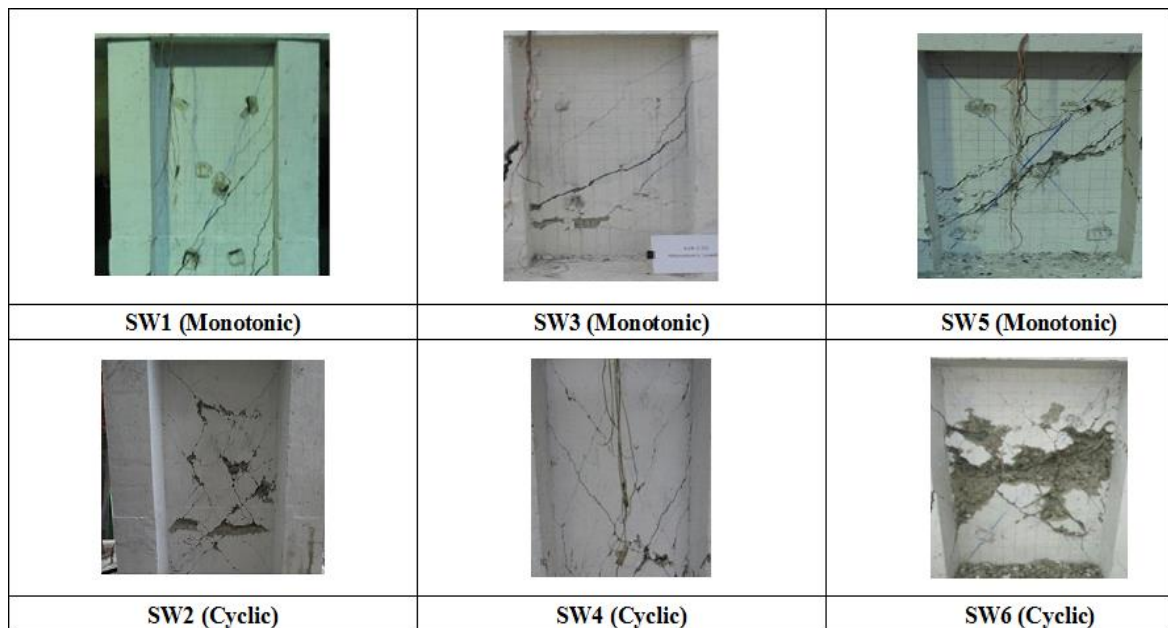


Fig. 4 Crack pattern in all the walls at ultimate load

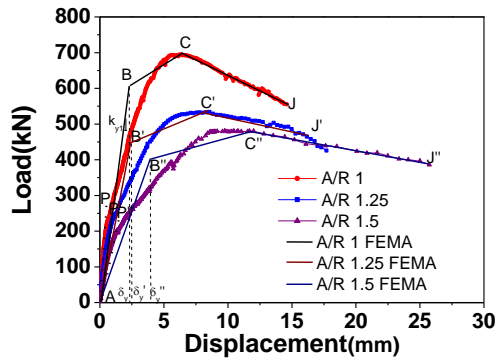


Fig. 5 Backbone curve for shear walls with various A/Rs obtained from tests

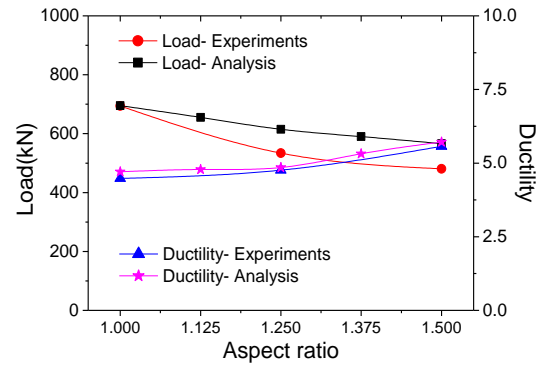
Table 2 Results of experiments

	Parameters Measured	1 st Shear Crack Point	Yield point	Ultimate /Peak Point	Failure Point
SW1- Mono A/R 1.5	Load (kN)	181	305	481	435
	Displ. (mm)	1	3.5	10.9	20
	Crack width (mm)	0.1	0.3	2.8	6.7
SW3- Mono A/R 1.25	Load (kN)	221	447	535	502
	Displ. (mm)	0.8	2.5	8.7	15.2
	Crack width (mm)	0.10	0.5	2.7	5.5
SW5- Mono A/R 1	Load (kN)	236	604	701	621
	Displ. (mm)	0.5	2.4	6.4	11.8
	Crack width (mm)	0.1	0.5	2.8	5

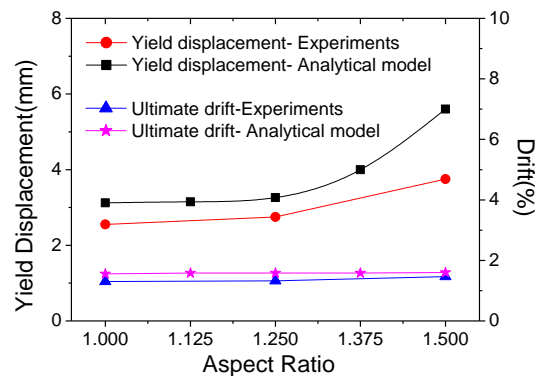
All the walls were essentially subjected to the intended in-plane action. The details of crack formation and results obtained are explained henceforth.

2.5.1 Crack formation

For all specimens, first flexural cracks initially appeared in the boundary elements near the bottom part of the tensile zone of the wall when only 20% of the wall capacity was reached. The first shear cracks in the wall panel were observed when 35 to 40% of load capacity is reached. As the cyclic lateral load approached nearly 60 per cent of its maximum value, significant inclined shear cracks were formed. The test loads and corresponding displacements for all the specimens for major states of diagonal cracking, yielding and ultimate are given in Table 2. After reaching the peak load, the length and width of the previously formed diagonal cracks were increased and the cracks were extended to the boundary elements. The crack pattern observed in all the walls at the end of the tests is shown in Fig. 4. It can be observed from Fig. 4 that for SW1, SW3 and SW5 specimens with aspect ratio 1.5, 1.25 and 1 respectively, there are major diagonal cracks in one direction. For SW2, SW4, SW6 cracks are formed in criss-cross pattern due to cyclic loads. For SW6 spalling of concrete in the middle section after reaching the ultimate load was observed. For this wall at the mid portion of wall web there was an intersection of diagonal cracks in both the directions and due to weak plane at mid portion, there was a major web crushing in the wall web. Initially diagonal



(a) Variation of ultimate load and ductility



(b) Variation of ultimate drift and yield displacements

Fig. 6 Variation of parameters of shear walls with A/Rs

cracks were developed but later failure was dominated by web crushing.

2.5.2 Strain gauge results

Strain gauge data from the structural testing of shear walls SW1 to SW6 were collected. The strain gauges were attached to the re-bars (as shown in Fig. 1) in the shear wall panels and not in boundary elements. In shear wall panel for walls of aspect ratio 1, 1.25 and 1.5 first the vertical reinforcement near the boundary element close to the bottom slab yielded at lateral displacement of 3 mm, 3.5 mm and 5 mm respectively. Subsequently, after the peak load was reached, horizontal rebar near the boundary element close to the bottom slab yielded for the walls of aspect ratio 1.25 and 1.5. Finally, just before the failure of each wall, vertical reinforcement close to the centre of wall panel yielded for the walls of aspect ratio 1 and 1.25.

2.5.3 Load displacement curves

The back bone curve of lateral load versus top displacement established from the tests for SW1, SW3 and SW5 specimens of different aspect ratios is shown in Fig. 5. Idealized force displacement relationship is obtained using FEMA 356(ATC-40) procedure. This relationship is bilinear, with initial slope K_1 and post-yield slope α for all the walls. In the present work tri-linear force displacement relationship (as shown in Fig. 5) with slope of softening portion of the curve after ultimate load is also defined. Idealized force-displacement curve is plotted using an iterative graphical procedure that approximately balances the area above and below the curve. The effective lateral

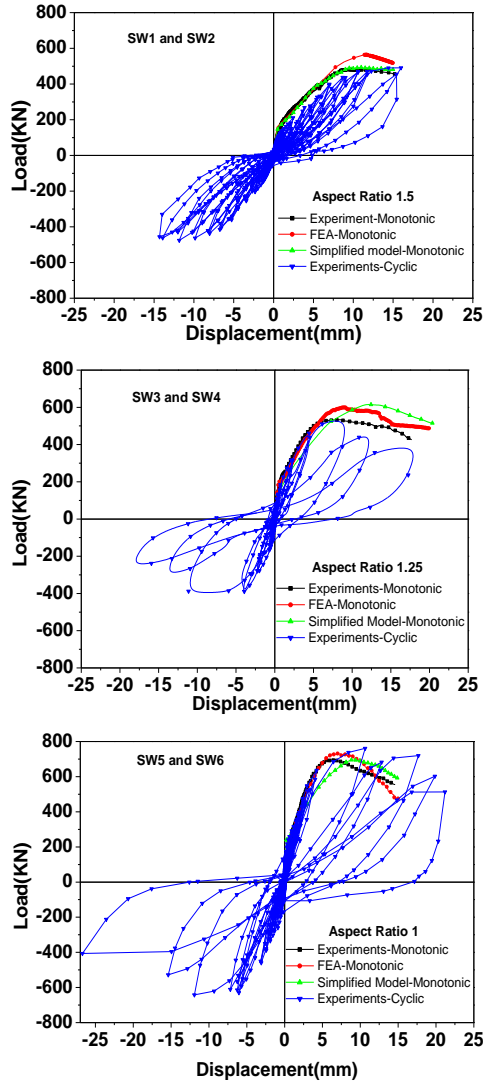


Fig. 7 Comparison of analysis and test results

stiffness, K_{y1} , shall be taken as the secant stiffness calculated at a base shear force equal to 60% of the effective yield strength of the shear wall as per FEMA-356 procedure. The yield displacements, the yield load of the shear walls, ultimate displacement and ultimate load are obtained from the initial bilinear portion of force displacement curve for shear walls with various aspect ratios. The displacement corresponding to softening region beyond ultimate load for the value of 85% of the ultimate load is defined as displacement at failure. The ultimate ductility of each shear wall is obtained as ratio of displacement at failure to yield displacement. The ultimate drift is the ratio of failure displacement to height of wall expressed in percentage. The results obtained from the tests in the form of the ultimate load and ductility with aspect ratio are plotted in Fig. 6(a). It is observed as that the ductility increases and the peak ultimate load of shear wall decreases with increase in aspect ratio from 1 to 1.5. The variation in the yield displacement and the ultimate drift (drift limit) at the top of the wall with the varying aspect ratio is plotted in Fig. 6(b). Drift limit statistics for shear walls was carried out by Duffy *et al.* (1993) and for walls

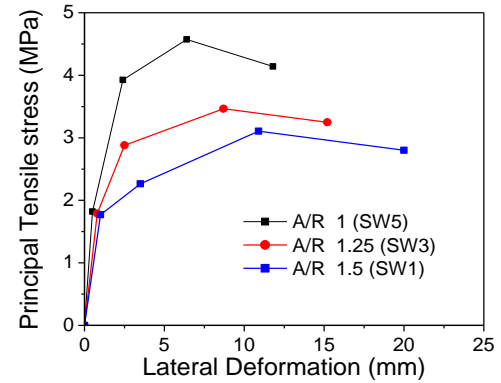


Fig. 8 Principal tensile stresses developed in the shear walls (Specimens: SW1, SW3, SW5)

with aspect ratio of 1, the median value of ultimate drift recommended by them is 1.15 %. The value of drift obtained in the present work for shear wall with aspect ratio of 1 is 1.5%. Thus the drift values obtained are in concurrence with the drift limit statistics carried out by Duffy *et al.* (1993). It is observed from the figures that as aspect ratio increases, the ductility increases however the drift remains same.

Fig. 7 shows the experimental results for cyclic load for SW2, SW4, and SW6. The test backbone curve for monotonic loading for same aspect ratio walls (SW1, SW3 and SW5 respectively) is also shown in the Fig. 7. It is observed that the monotonic tests results envelopes the cyclic except in case of wall of aspect ratio 1.0 (SW6) as observed in Fig. 7. It is observed from Fig. 7 that the cyclic load displacement results are slightly higher than monotonic. This is because the cube strength of concrete for SW6 is higher than other walls by 10 %. (See Table 1).

2.5.4 Evaluation of test results

The test results of the specimens are utilized to evaluate their performance in terms of computation of principal stresses developed, energy dissipation in hysteretic deformation and evaluation of damage index. Evaluation of all these parameters for the tested specimens facilitates in understanding thoroughly the performance of the RC wall assemblages during seismic load.

Principal tensile stresses

The cracking and damage to the shear walls occur due to the principal tensile stresses developed in the shear walls due to applied constant axial load and increasing shear loads till their failure. The nominal principal tensile stresses developed in three shear walls subjected to monotonic load (SW1, SW3 and SW5) are obtained for major states of diagonal cracking, yielding, ultimate and failure. Fig. 8 demonstrates the nominal principal tensile stresses values developed in the wall panel region for the three shear walls of aspect ratio 1, 1.25 and 1.5. It can be deduced from the figure that the principal tensile stresses developed in wall of aspect ratio 1 at ultimate load is the highest and is equal to $1.02\sqrt{f_c}$. The principal tensile stress developed in the shear wall with aspect ratio 1.5 at ultimate load is equal to $0.68\sqrt{f_c}$.

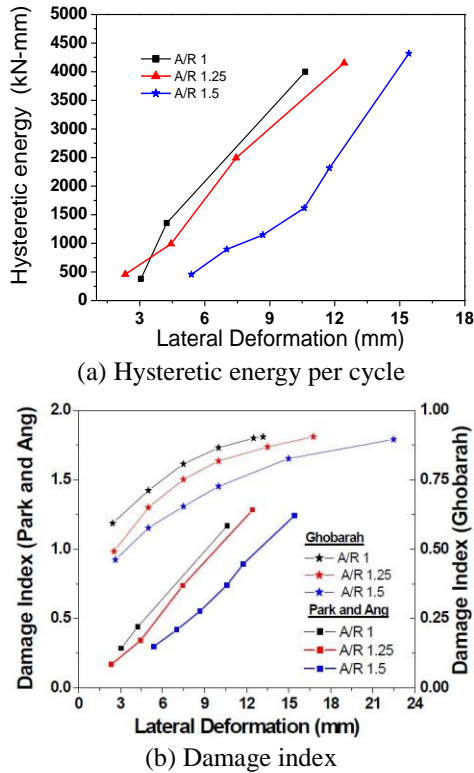


Fig. 9 Hysteretic energy per cycle and damage index v/s lateral deformation

Hysteretic energy dissipation

Energy dissipation represents the capacity of the specimen to be stressed until failure and gives the important parameter of damping for evaluation of dynamic response. The energy dissipated by each shear wall specimen (SW2, SW4 and SW6) due to cyclic load is evaluated by calculating the area enclosed by the hysteretic loops of the load displacement curves for that particular displacement. Thus, the energy dissipated for each cycle is obtained and plotted corresponding to the lateral deformation for each shear wall as depicted in Fig. 9(a). It is observed that for a particular lateral displacement the energy dissipation of shear wall decreases as aspect ratio increases. However, it is observed that for a particular state of deformation of the shear walls say ultimate state, the deflection of shear walls of A/R 1, 1.25 and 1.5 are 6 mm, 9 mm and 12 mm respectively as shown in Fig. 7. For this ultimate state of deformation, the energy dissipated by shear walls of A/R 1, 1.25 and 1.5 respectively are 2000 kN-mm, 2500 kN-mm and 2600 kN-mm (Fig. 9(a)). Similarly, for deformation at failure point the energy dissipation of shear walls of A/R 1, 1.25 and 1.5 are 4000 kN-mm, 4150 kN-mm and 4300 kN-mm respectively. Hence, it is observed that the energy dissipation is in increasing order with increasing aspect ratio of the shear walls for a particular state of damage. The damping evaluated at ultimate drift of the walls ranges between 15 to 20%.

Damage index

A damage index is used as an indicator to describe the state of the lateral load-carrying capacity and the reserve

capacity of the structural components or structures. In this study, the model by Park and Ang (1985) is employed for evaluation of damage index for the SW2, SW4 and SW6 specimens subjected to cyclic loads. As per this damage model, the seismic structural damage is a linear combination of the damage caused by excessive deformation and the damage accumulated by repeated cyclic loading effect. The Park-Ang damage index combining both ductility and cumulative hysteretic energy demand is given by the following equation

$$D_{PA} = \frac{\delta_m}{\delta_u} + \frac{\beta}{\delta_u F_y} \int dE_h \quad (1)$$

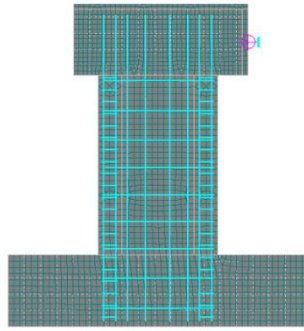
where δ_m is the maximum deformation under earthquake, δ_u is the ultimate deformation under monotonic loading, F_y is the yield strength, dE_h is the incremental absorbed hysteretic energy and β is the non-negative parameter representing the effect of cyclic loading on structural damage. The quantitative estimation of coefficient β was made by researchers by conducting extensive experimentations and the results reported a median value of β of about 0.15 (Cosenza *et al.*). It is mentioned that the value of $\beta=0.15$ correlates closely with the results of other damage models, and this value has widely been adopted by the researchers. Hence, in this study the value of β is considered as 0.15. A perfect damage index typically normalizes the damage on a scale of 0 to 1, where zero represents undamaged state while unity represents the collapse state of the structure/component. The maximum value of the Park-Ang damage index is over 1 and nearly close to 2 in some cases. In addition, the Park-Ang damage index is not directly suitable for nonlinear static pushover analysis as the cumulative damage does not occur in this case. Based on pushover analysis, a stiffness damage index was presented by Ghobarah (2001) as given by the following equation

$$D_k = 1 - \frac{k_f}{k_i} \quad (2)$$

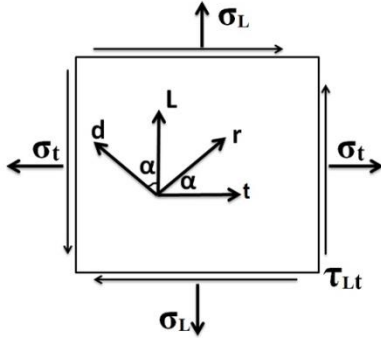
Where k_i is the initial slope of the pushover curve of the structure/component before subjecting it to the earthquake ground motion and k_f is the slope of the same relationship but after subjecting the frame to the earthquake time history. The values of these damage indices given by Ghobarah range from zero to one depending on the amount of damage experienced. The calculated damage indices based on the above described Park and Ang model and Ghobarah model are presented in Fig. 9(b). These damage indices are compared for all the shear walls in the figure. It is observed from the figure that the damage index by Ghobarah reaches a value of 0.88 for all the walls at ultimate drift which signifies the damage degree of collapse. It can be concluded from the results of Park and Ang damage index evaluated for the three shear walls that maximum damage index value of 1.25 is reached at ultimate displacement.

3. Simulation

Analytical simulation of the shear walls for monotonic



(a) Shear wall of aspect ratio 1.5



(b) Stress condition in an element of the shear wall

Fig. 10 FE model

lateral loads is carried out using FE analysis and a simplified truss model, considering flexure-shear interaction to evaluate the backbone curve. Moreover, a simplified hysteretic model is suggested based on the experimental cyclic characteristics for shear walls.

3.1 FE Modelling and analysis

Concrete with nonlinear material properties is modelled using four noded iso-parametric 2D plane quadrilateral elements for the shear wall, top beam and bottom beam. Reinforcing steel provided in the wall is modelled as discrete form of truss element. In the top beam and bottom beam reinforcement is modelled in smeared form. The finite element model of shear wall SW1 of 1m width, 1.5 m height and 0.15 m thickness is as shown in Fig. 10(a). The cube compressive strength of concrete and tensile strength of steel is considered as per Table 1 (28 days strength) for SW1. The ratio of cylinder to cube strength is considered as 0.81. The axial load of 6 tons was applied on the FE model as applied during test.

FE analysis of the shear wall is carried out by simulating the test boundary conditions of the foundation as fixed in all directions. For the top beam all the translations and rotations were set free except translation in the direction, for which a fixed displacement was defined as the loading condition. Steel plates with less (fictitious) density are attached to 3 sides of top beam so that there is no local failure in the top beam due to point load application. Nonlinear concrete model is considered. Kent and Park (1971) concrete material model is chosen for the analysis which includes non-linear behaviour in compression including hardening and softening. Fracture of concrete in tension is based on the nonlinear fracture mechanics. The biaxial strength failure criterion, reduction of compressive

strength after cracking, tension stiffening effect and reduction of the shear stiffness after cracking is also considered in the model. The reduction of compressive strength after cracking shown by factor β is considered as 0.45. The steel is modelled as reinforcement bars with a bilinear elastic-plastic model. Nonlinear analysis is carried out for monotonic and cyclic load on the wall with constant axial load of 6 tons. Analysis is carried out according to the loading protocol given in the experiment till failure of the wall i.e., the load drops to 85% of ultimate peak load. Comparison of experimentally obtained and analytically simulated backbone curve is shown in Fig. 7.

3.2 Simplified truss model

Shear-flexure interaction of shear wall with aspect ratio 1 to 1.5 should be essentially considered while determining the force displacement characteristic of shear wall. Simplified truss model is described which combines the shear with flexure characteristics and analytical force displacement relationship is obtained. Shear characteristics of the shear wall is determined using the widely accepted procedure of softening truss approach given by Vecchio and Collins (1986). Cracked reinforced concrete in compression has been observed to exhibit lower strength and stiffness when compared to uniaxially compressed concrete. There is reduction of the compressive strength in one direction by cracking, due to tension in the perpendicular direction. This aspect is taken care in the concrete nonlinear model. Concrete model comprises non-linear compressive behaviour that is capable of modelling, hardening and softening characteristics. The pre-peak relation is based on the equation of quadratic parabola (Kollegger and Mehlhorn 1990) given below. Thus when $\varepsilon < \varepsilon_0$ then

$$\sigma = f'_c \left[\frac{2\varepsilon}{\varepsilon_0} - \left(\frac{\varepsilon}{\varepsilon_0} \right)^2 \right] \quad (3)$$

where ε is the compressive strain in concrete and ε_0 is the compressive strain corresponding to peak cylindrical compressive stress, f'_c . The ratio of cylinder to cube compressive strength is considered as 0.81. The value of ε_0 used in the analysis is 0.002 based on literature. The post peak compressive behavior is linear descending, and the slope of the softening law is defined by means of the softening modulus E_d such that f'_c is reduced to zero at $4.7\varepsilon_0$. This value is given for short shear wall (Parulekar *et al.* 2014). Thus, the post peak behavior is defined by relation

$$\sigma = f'_c + E_d(\varepsilon - \varepsilon_0) \quad (4)$$

Moreover, compressive strength in the direction parallel to the cracks is reduced considering a modification factor β to reduce the peak stress of the stress strain curve of concrete in which the base curve is modified by peak stress only. The factor β suggested by Vecchio and Collins (1994) is given by following relation

$$\beta = \frac{1}{1 + K_c K_f} \quad (5)$$

Where, K_c represents effect of transverse cracking and K_f represents dependence on strength of concrete.

$$K_c = 0.27 \left(\frac{\varepsilon_r}{\varepsilon_0} - 0.37 \right) \quad (6)$$

$$K_f = 0.1825 \sqrt{f'_c} \quad (7)$$

Where ε_r is the principal tensile strain.

The softening model used for obtaining the shear spring characteristics consists of diagonal concrete compression struts and the equilibrium and compatibility equations are explained henceforth. Fig. 10(b) shows a concrete element in the stationary $l-t$ coordinate system, defined by the directions of the longitudinal and transverse steel and rotated $d-r$ co-ordinate system with rotation angle α . When a concrete element is reinforced orthogonally with longitudinal and transverse steel bars, the three stationary stress components, σ_l , σ_t and τ_{lt} are the applied stresses on the element. The stresses in the longitudinal and transverse steel are denoted by $\rho_l f_l$ and $\rho_t f_t$ respectively, where ρ_l and ρ_t are reinforcement percentages in l and t axes respectively. The reinforcement stress strain relationship is defined by the bilinear law in which elastic-plastic behavior is assumed. Hence from the super position principle

$$\sigma_l = \sigma_d (\cos \alpha)^2 + \sigma_r (\sin \alpha)^2 + \rho_l f_l \quad (8)$$

$$\sigma_t = \sigma_r (\cos \alpha)^2 + \sigma_d (\sin \alpha)^2 + \rho_t f_t \quad (9)$$

$$\tau_{lt} = (-\sigma_d + \sigma_r) \cos(\alpha) \sin(\alpha) \quad (10)$$

The same principle of transformation for stresses can be applied to strains considering ε_r as principal tensile strain and ε_d as principal compressive strain. Therefore, the following compatibility equations can be derived.

$$\varepsilon_l = \varepsilon_d (\cos \alpha)^2 + \varepsilon_r (\sin \alpha)^2 \quad (11)$$

$$\varepsilon_t = \varepsilon_r (\cos \alpha)^2 + \varepsilon_d (\sin \alpha)^2 \quad (12)$$

$$(\gamma_{lt}/2) = (\varepsilon_d + \varepsilon_r) \cos(\alpha) \sin(\alpha) \quad (13)$$

For framed wall panel the strain of transverse steel in low-rise shear walls can be neglected $\varepsilon_t=0$ and the tensile strength of concrete is neglected, $\sigma_r=0$. Shear deformation characteristics of the shear wall can be thus obtained by solving Eq. (8) to Eq. (10) and Eq. (11) to Eq. (13). Neglecting the tensile stress in concrete element and considering σ_r as zero, the unknowns in the equations are ε_d , ε_l , σ_d and α . The step by step procedure is used for evaluating these variables and obtaining the shear deformation characteristics by simplified softening strut approach.

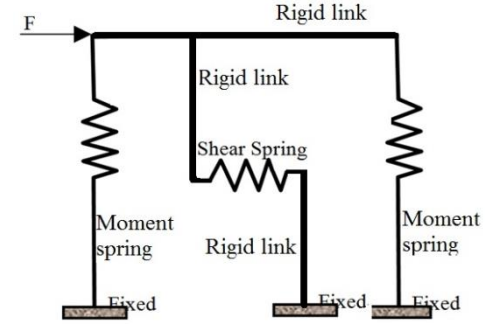
Initially assuming small value of ε_d and value of α as 45° , the above equations are used and iteratively the force v/s displacement relationship for the shear wall is obtained from shear characteristics using following equations

$$\text{Shear force } V = \tau_{lt} * t_w * d_w \quad (14)$$

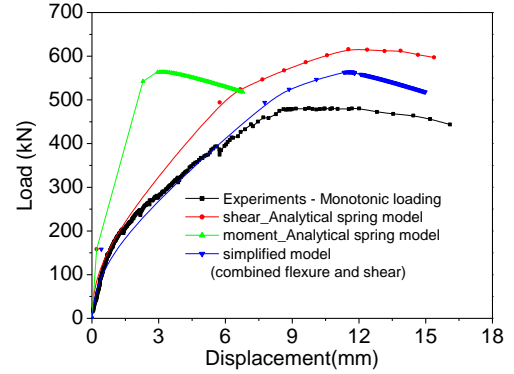
$$\text{Displacement } \Delta = \gamma_{lt} * H_w \quad (15)$$

Where t_w , d_w and H_w are thickness, depth and height of the shear wall respectively.

The aspect ratio of the wall specimens is varying from short to mid-rise with small axial compression. Therefore, failure of the shear wall is also governed by flexural yielding and the evaluation of flexural strength of the shear wall is based on the basic principles of beam with axial



(a) Moment shear spring model



(b) Load displacement response (A/R1.5)

Fig. 11 Simplified spring model

load. The nonlinear behaviour of a beam depends primarily on its moment-rotation behavior, which in turn depends on the moment-curvature characteristics of the plastic hinge section and the length of the plastic hinge. The moment-curvature ($M-\phi$) characteristics of RC sections of the shear wall is developed using the widely used Kent and Park model (Kent and Park 1971) for concrete and elastic perfectly plastic model for steel. The ductile design provisions of IS 13920 require that transverse reinforcements in beams and columns should be able to confine the concrete core. Thus, if the stirrups are provided using IS13920 then the Kent and Park model for confined concrete is used for modeling the concrete within the stirrups. However, if the stirrups are laid far off without IS 13920 provisions then the unconfined concrete characteristics, following again the Kent and Park guidelines are assigned for the concrete model. Priestley (1997) prescribed an ultimate concrete strain (in compression) for unconfined concrete, $\varepsilon_{cu}=0.005$, which is adopted in the present work to obtain moment curvature of the shear walls.

For the three shear walls of aspect ratios 1, 1.25 and 1.5 with specifications and material properties as given in Table 1, the moment curvature relation is obtained. The maximum displacement of the shear wall is calculated for particular load from moment curvature relationship using principle of virtual work thus load displacement relation is obtained. A simplified truss model of the shear wall is shown in Fig. 11(a). The shear spring and moment spring are connected in series. The load displacement relationship obtained thus from the moment curvature relationship for shear wall of aspect ratio 1.5 is shown in Fig. 11(b). The load

displacement relation obtained from shear characteristics for the same shear wall is shown in Fig. 11(b). The combined load displacement relationship obtained by considering the flexure and shear springs in series is shown for shear wall with aspect ratio 1.5 in Fig. 11(b) and is denoted as simplified model. The load-displacement relation of the simplified truss model is matching with the test results of the shear wall till pre-peak perfectly. In the post-peak region, the load values of simplified model are slightly higher than that of test results.

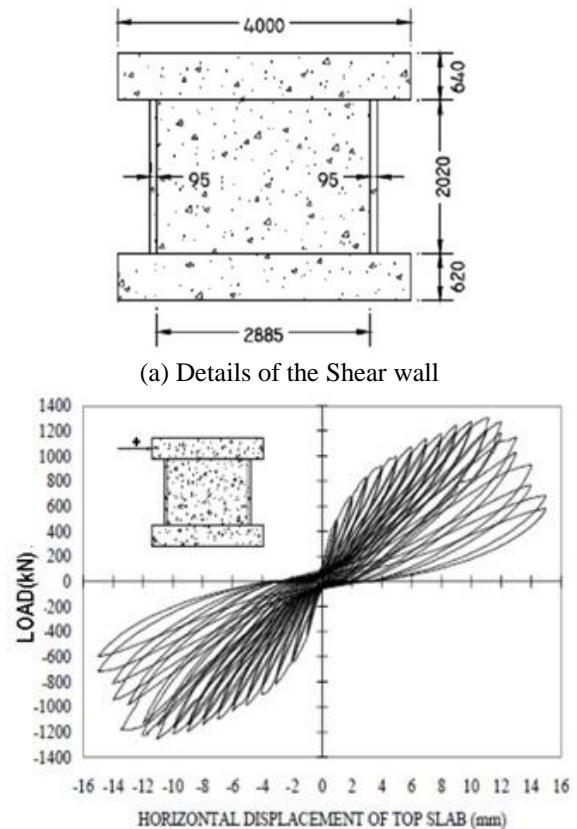
In a similar way, combined flexure and shear characteristics are obtained and the simplified model force displacement curve (backbone curve) is obtained for the other shear walls with aspect ratio 1 and 1.25. The comparison of the backbone curves for all the three shear walls with tests, simplified model and FE analysis using 2D element is shown in Fig. 7. It is observed that there is good agreement in the curves. Also, the ductility, ultimate load, yield displacement and drift of all shear walls are calculated based on the simplified model and compared with tests as shown in Fig. 6(a) and 6(b).

3.3 Hysteretic model

Evaluation of nonlinear response of shear walls for earthquake loads requires nonlinear dynamic analysis to be carried out. If nonlinear dynamic analysis is carried out using 2D FE model, it will require large computational efforts. Hence it is necessary to define a multi-linear cyclic hysteretic spring model which will be very effective to accurately predict the cyclic response of shear wall with less computational efforts. Earlier, in literature (Takeda 1970, Otani 1974, Saiidi and Sozen 1988, Lestuzzi *et al.* 2003) many hysteretic models were used. These models were based on the parameters of RC walls like initial stiffness, the yield displacement, the post yield stiffness, a parameter relating the stiffness degradation and another parameter specifying the target for the reloading curve. Moreover, different rules are used for large and for small hysteretic cycles. However, the maximum force and displacement factors depending on ductility and pinching point were not included to form the hysteretic rules. This paper discusses a multi-linear hysteretic model for lightly reinforced (horizontal and vertical reinforcement between 0.3 to 0.75%) short shear walls with axial load ratio of less than 5%.

Three numbers of shear walls of aspect ratio 1, 1.25 and 1.5 tested for cyclic load with the hysteretic characteristics shown in Fig. 7 are considered to propose the model. Moreover, two more shear walls tested by Palermo and Vecchio (2002), Greifenhagen and Lestuzzi (2005) with schematic and hysteretic curves shown in Figs. 12 and 13 respectively were considered to evaluate the analytical model parameters. The details of the shear walls are given in Table 3

Initially, the analytical backbone curves of the shear walls are evaluated by the methodology given in section 3.2. The analytical backbone curve obtained using this methodology is in good agreement with monotonic loading tests results (Fig. 7). Using these backbone curves five parameters of the hysteretic model are defined namely the yield stiffness, the yield displacement, the post yield stiffness, ultimate/peak load and stiffness after peak. Fig. 14 shows the multi-linear hysteretic model in which slope AB



(b) Experimental Load Displacement curve

Fig. 12 Shear wall (Palermo and Vecchio 2002)

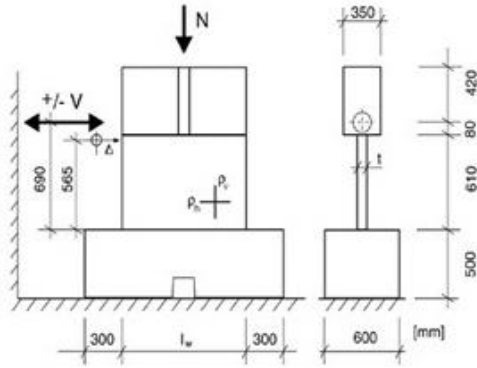
is the yield stiffness, δ_y is the yield displacement, slope BC is the post yield stiffness, load corresponding to point C denotes ultimate/peak load and slope CJ is the stiffness after peak. The actual slope of branch CJ obtained from tests of short walls (shown in Fig. 5) showed decreasing shear strength with increasing displacement. However, in the proposed model branch CJ (Fig. 14) of the model is taken as nearly constant maintaining the actual ultimate/failure displacement obtained from tests. In order to characterize the unloading part of the hysteretic curves the stiffness degradation parameter is defined. This stiffness degrading parameter is given as function of initial pre-cracking stiffness of the wall. The initial pre-cracking stiffness, k_i of the wall is obtained from tests (shown in Fig. 5 as slope AP) or by backbone curves obtained from analysis methodology explained in section 3.2. The reduction in the unloading stiffness represent the damage occurred in the shear wall and this unloading stiffness goes on decreasing with increase in ductility of the wall as number of cycles increase and the corresponding damage increases. The unloading stiffness degradation factor, c which is the ratio of reduced unloading stiffness to the initial stiffness (pre-cracking stiffness) is plotted with ductility for different aspect ratios (Fig. 15(a)) from experiment conducted for short walls in the current work and literature.

When unloading occurs at any n th level of displacement greater than yield displacement, the stiffness can be given as

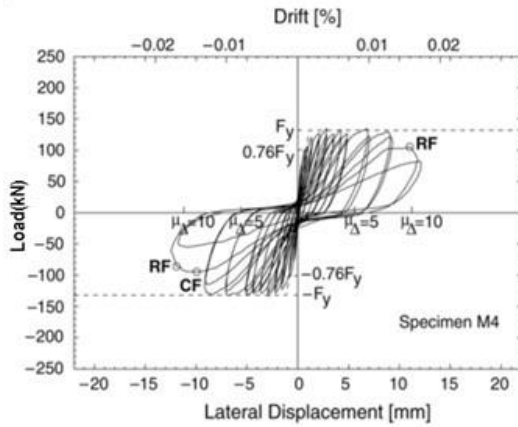
$$k_n = c k_i \quad (16)$$

Table 3 Details of Shear walls tested in Literature

Experiments by	A/R	web thickness (mm)	$f'c$ (MPa)	F_y (MPa)	% steel in web ρ_h	% steel in web ρ_v	% steel in flanges ρ_h	% steel in flanges ρ_v	Axial load ratio (%)
Palermo and Vecchio	0.7	75	22	605	0.73	0.79	0.58	0.627	5
Greifenhagen and Lestuzzi	0.67	80	24.4	605	0.3	0.3	N.A	N.A	5



(a) Details of the shear wall



(b) Experimental load displacement curve

Fig. 13 Shear wall (Greifenhagen and Lestuzzi 2005)

This parameter, c depend on ductility, μ and is given by the equation

$$c = 0.0167\mu^2 - 0.196\mu + 0.85 \quad (17)$$

Finally, the pinching effect observed in low rise shear walls needs to be accurately modelled which gives rise to lesser damping and thus higher dynamic response than that observed for high rise shear walls. The location of the pinching points E and I in the hysteretic model shown in Fig. 14 are obtained by defining the abscissa and ordinate of each pinching point. The ordinate of each pinching point is determined by the maximum force factor, γ and the abscissa of each pinching point is determined by the permanent deformation factor, λ .

Thus, as shown in Fig. 14, during reverse cyclic load, the force (the ordinate) in pinching point is governed by the product of force factor and maximum force in previous cycle (F_{max}) or yield force, F_y whichever is higher. Moreover, the displacement (abscissa) in the pinching point is governed by product of displacement factor, λ and the maximum permanent deformation in the previous cycle, δ_p where δ_p is equal to $(\delta_{max} - \delta_y)$. For example, in case of pinching point, E as the yielding force is still not reached and permanent deformation

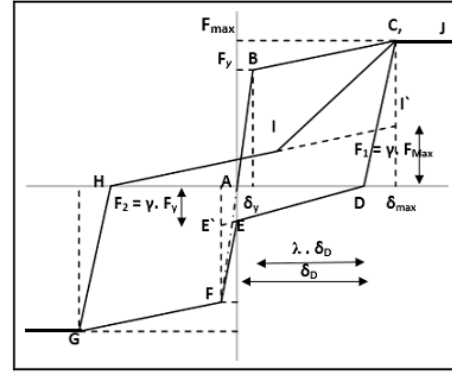
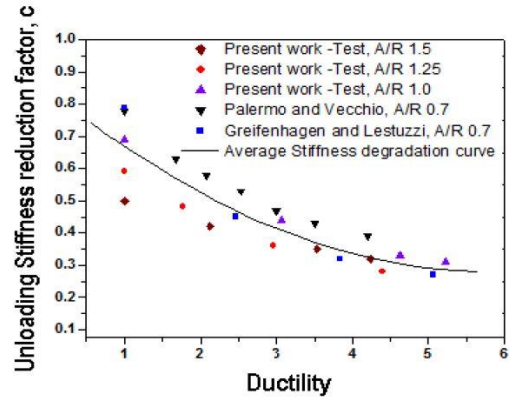
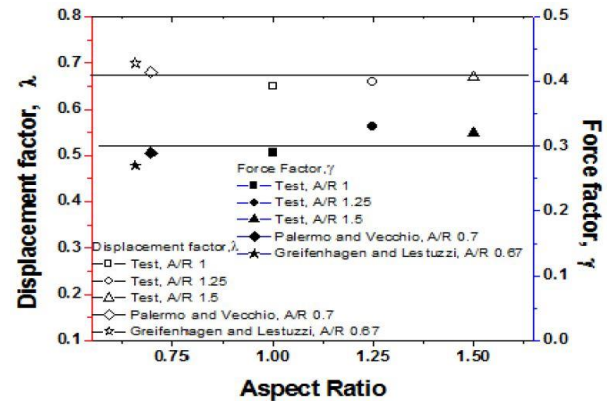


Fig. 14 Proposed multi-linear model of shear wall



(a) Variation of unloading Stiffness degradation with Ductility



(b) Displacement and force Pinching factors

Fig. 15 Parameters for different aspect ratios of shear walls

in that direction is zero, the abscissa of the pinching point E is zero. The ordinate of point E is obtained by first locating point E' with ordinate, γF_y and abscissa, δ_y as shown in Fig. 14 and then obtaining the slope of DE' . Similarly, in order to locate the pinching point, I the abscissa of pinching point I is obtained as $(\delta_{max} - \lambda \delta_p)$. The ordinate of the pinching point, I is obtained by first locating point I' with ordinate, γF_{max} and abscissa, δ_{max} and

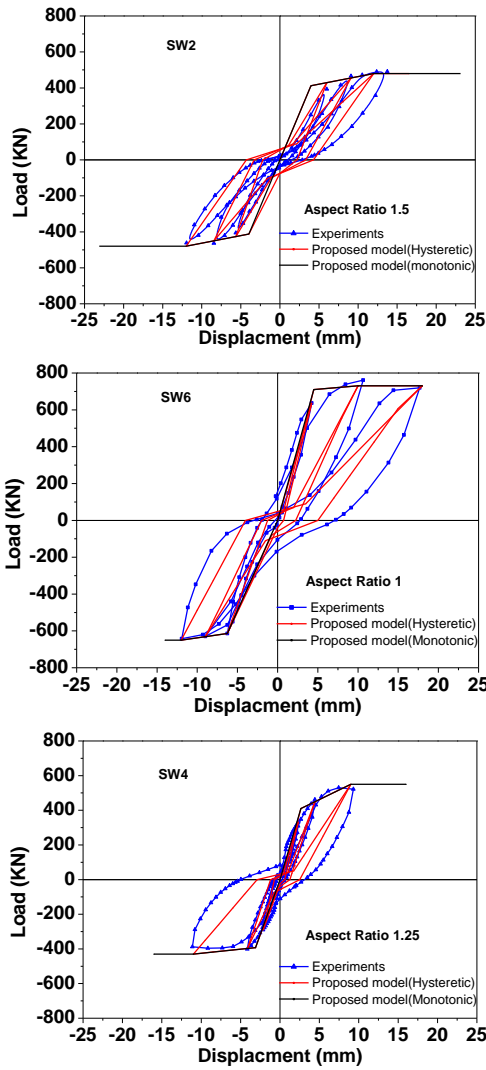


Fig. 16 Validation of proposed model with cyclic test results of shear walls

then obtaining the slope of HI'.

The value of force factor, γ and permanent deformation factor, λ obtained from tests performed in literature and the 3 walls tested in present work is shown in Fig. 15(b). For all the walls, considering the average, the force factor, γ is obtained as 0.3 and displacement factor, λ is obtained as 0.675. The proposed analytical model is explained for different paths of hysteretic rules from Fig. 14,

Elastic (loading), Path A-B

$$F(t) = k_{y1}x(t) \quad (18)$$

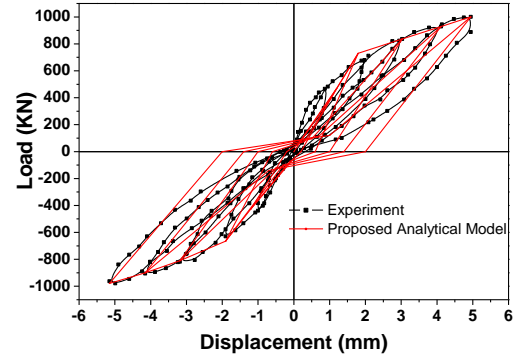
Post yield deformation (loading), Path B-C

$$F(t) = F_y + k_{y2}(x(t) - \delta_y) \quad (19)$$

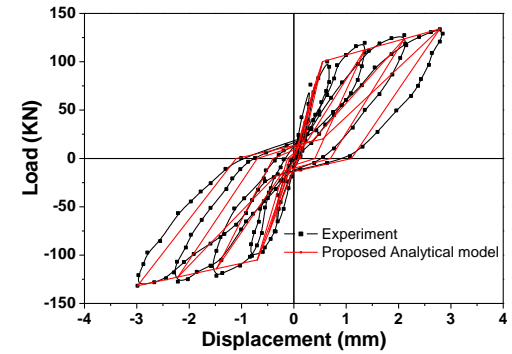
Where K_{y1} , K_{y2} are the pre and post yield stiffness respectively, F_y is the yield force and δ_y is the yield displacement.

Path C-D (where displacement and force at C is δ_{max} and F_{max} respectively)

or Path G-H, (where the displacement and force at G are



(a) Palermo and Vecchio (2002)



(b) Greifenhagen and Lestuzzi (2005)

Fig. 17 Validation of proposed model with cyclic test results of shear walls tested in literature

δ_{min} and F_{min} respectively)

$$F(t) = F_{max} + k_1(x(t) - \delta_{max}) \quad (20)$$

Where, k_1 is obtained from Eq. (16) and value of c from Eq. (17) at ductility value of $\mu = \delta_{max}/\delta_y$.

For the path D-E-F

Point 'E' acts as a pinching point whose position depends on the maximum permanent deformation and load experienced in that direction of loading. The abscissa of the point E is zero and that of E' is δ_y .

Thus, the ordinate of the pinching point E is

$$F_E = [\gamma F_y / (\delta_y + \delta_D)] \times (\delta_D) \quad (21)$$

Using this Eq. (21), abscissa and ordinate of pinching point, E and consequently the force in path DE can be obtained. Similarly, for path HI the abscissa of the pinching point (point I) is defined by the parameter λ , and is given by $(\delta_{max} - \lambda \delta_D)$. The ordinate of point I' is γF_{max} and abscissa of point I' is δ_{max} . Thus, and the ordinate of pinching point I is given by the equation

$$F_I = \{(\gamma F_{max}) / (\delta_{max} - \delta_{min} - \delta_y)\} \times (\delta_{max} - \lambda \delta_D - \delta_{min} - \delta_y) \quad (22)$$

Where, δ_{min} is the minimum displacement at point G and it is -ve in value. Using this Eq. (22) abscissa and ordinate of pinching point I, and consequently the force in path HI can be obtained. Once the pinching point (E and I) is reached, the reloading path is directed towards the maximum deformation of previous cycles in the direction of loading or the yield displacement whichever is larger. Thus,

the slopes of part *EF* and *IJ* will depend on the pinching points and the maximum deformation of previous cycles in that direction.

For low rise shear walls of aspect ratio less than 1.5 the multi-linear model can be obtained by considering stiffness degradation parameter from Eq. (17) and choosing γ as 0.3 and λ as 0.675, the validation of the proposed analytical multi-linear model is shown in Fig. 16 for wall of aspect ratio 1.5, 1.25 and 1 respectively.

Similarly, hysteretic characteristics of analytical model are generated for tests carried out in literature, by Palermo and Vecchio (2002), Greifenhagen and Lestuzzi (2005) for wall of aspect ratio 0.7 and 0.67 respectively. The comparison of test hysteresis and hysteresis generated by proposed analytical model is shown in Fig. 17(a) and 17(b). The hysteretic curve from the analytical model is in good agreement with test results for shear walls tested in present work and tested by researchers in literature. Thus, the proposed multi-linear hysteretic model can be used effectively.

4. Conclusions

In the present work, experimental results of six low rise lightly reinforced shear walls of aspect ratio 1 to 1.5 with axial load ratio of 1% are presented in order to evaluate the backbone curves, stiffness degradation and pinching factors and utilize these factors for generation of analytical model. These factors are also evaluated from two similar shear walls tested in literature. Based on the results of the experimental program and the analytical model following conclusions are drawn.

- Experimental results performed on the walls demonstrate that shear walls produce highly pinched hysteresis curve and are greatly influenced by shear related mechanisms and same is obtained using 2D FE analysis.
- The shear wall with aspect ratio 1.5 shows the lowest wall capacity (lesser by 30 % than that of aspect ratio 1) as the wall capacity is affected by the flexural as well as shear strength of the specimen. However, the ductility of shear wall with aspect ratio 1 is the lowest (lesser by 25 % than that for aspect ratio 1.5) due to predominant brittle shear failure.
- The hysteretic energy dissipated for the walls of aspect ratio 1.5 is higher than that of the walls of aspect ratio 1 and 1.25 for particular state of damage in the walls such as yielding, ultimate and collapse. The damping evaluated at the failure displacement from the dissipated hysteretic energy lies in the range of 15 to 20 %.
- The Park and Ang damage index evaluated for all the three walls reaches a maximum value of 1.25 at failure displacement which is defined as displacement at which peak load drops to 85 % of ultimate load. The damage index based peak to peak on stiffness degradation given by Ghobarah is evaluated and at ultimate displacement this damage index reaches a value of 0.88 which signifies the damage degree of collapse.
- The analytical model for backbone curve is obtained using equilibrium equations and it accurately predicts

the pre and post peak region of the load deflection curve of short shear wall with aspect ratio 1,1.25 and 1.5. The multi-linear hysteretic model matches with experiments and can be used effectively for evaluation of nonlinear dynamic response of shear wall using a spring/truss model. The proposed model captures the global failure mode of shear walls however fails to capture some important three-dimensional effects such as the spalling observed in the specimens during the experiments.

References

- Beko, A., Rosko, P., Wenzel, H., Pegon, P., Markovic, D. and Molina, F.J. (2015), "RC shear walls: full-scale cyclic test, insights and derived analytical model", *Eng. Struct.*, **102**, 120-131.
- Brun, M., Labbe, P., Bertrand, D. and Courtois, A. (2011), "Pseudo-dynamic tests on low-shear walls and simplified model based on the structural frequency drift", *Eng. Struct.*, **33**, 769-812.
- Brun, M., Reynouard, J.M. and Jezequel, L. (2003), "A simple shear wall model taking into account stiffness degradation", *Eng. Struct.*, **25**, 1-9.
- Christidis, K.I. and Trezos, K.G. (2017), "Experimental investigation of existing non-conforming RC shear walls", *Eng. Struct.*, **140**, 26-38.
- Cosenza, E., Manfredi, G. and Ramasco, R. (1993), "The use of damage functionals in earthquake engineering: a comparison between different methods", *Earthq. Eng. Struct. Dyn.*, **22**, 855-868.
- Duffey, T.A., Goldman, A. and Farrar, C.R. (1993), "Shear wall ultimate drift limits", USNRC, NUREG/CR-6104.
- FEMA-356 (2000), Pre-Standard and Commentary for the Seismic Rehabilitation of Buildings, ASCE, Virginia, U.S.A.
- FEMA-461 (2007), Interim Testing Protocols for Determining the Seismic Performance Characteristics of Structural and Nonstructural Components, ASCE, Virginia, U.S.A.
- Feng, D.C., Ren, X.D. and Li, J. (2018), "Cyclic behavior modeling of reinforced concrete shear walls based on softened damage-plasticity model", *Eng. Struct.*, **166**, 363-375.
- Ghobarah, A. (2001), "Performance-based design in earthquake engineering: state of development", *Eng. Struct.*, **23**(8), 878-884.
- Greifenhagen, C. and Lestuzzi, P. (2005), "Static cyclic tests on lightly reinforced concrete shear walls", *Eng. Struct.*, **27**(11), 1703-1712.
- Habibi, F., Sheikh, S.A., Vecchio, F. and Panesar, D.K. (2018), "Effects of alkali-silica reaction on concrete squat shear walls", *ACI Struct. J.*, **115**(5), 1329-1339.
- IS 13920 (1993), Ductile Detailing of Reinforced Concrete Structures Subjected to Seismic Forces-code of Practice, Bureau of Indian Standards, New Delhi, India.
- Jeong, S.H. and Jang, W.S. (2016), "Modeling of RC shear walls using shear spring and fiber elements for seismic performance assessment", *J. Vib.*, **18**(2), 1052-1059.
- Kent, D.C. and Park, R. (1971), "Flexural members with confined concrete", *J. Struct. Div., Proc. of the American Society of Civil Engineers*, **97**(ST7), 1969-1990.
- Kollegger, J. and Mehlhorn, G. (1990), "Material model for the analysis of reinforced concrete surface structures", *Comput. Mech.*, **6**(5-6), 341-357.
- Kotronis, P., Ragueneau, F. and Mazars, J. (2005), "A simplified modelling strategy for R/C walls satisfying PS92 and EC8 design", *Eng. Struct.*, **27**(8), 1197-1208.
- Lestuzzi, P. and Badoux, M. (2003), "The gamma-Model: A simple hysteretic model for reinforced walls", Paper no 126, *Proceedings of the fib-Symposium: Concrete Structures in*

- Seismic Regions*, Athens, Greece.
- Lopes, M.S. (2001), "Experimental shear-dominated response of RC walls Part I: Objectives, methodology and results", *Eng. Struct.*, **23**, 229-239.
- Lopes, M.S. (2001), "Experimental shear-dominated response of RC walls Part II: Discussion of results and design implications", *Eng. Struct.*, **23**, 564-574.
- Otani, A. (1974), "Inelastic analysis of R/C frame structures", *J. Struct. Div.*, ASCE, **100**, 1433-1449.
- Palermo, D. and Vecchio, F. (2002), "Behavior of three dimensional reinforced concrete shear walls", *ACI Struct. J.*, **99**(1), 81-89.
- Park, R. and Ang, A.H.S. (1985), "Mechanistic seismic damage model for reinforced concrete", *J. Struct. Eng.*, ASCE, **111**(4), 722-739.
- Parulekar, Y.M., Reddy, G., Singh, R.K., Gopalkrishnan, N. and Ramarao, G.V. (2016), "Seismic performance evaluation of mid-rise Shear Walls: experiments and analysis", *Struct. Eng. Mech.*, **59**(2), 291-312.
- Parulekar, Y.M., Reddy, G.R., Vaze, K.K., Pegon, P. and Wenzel, H. (2014), "Simulation of reinforced concrete short shear wall subjected to cyclic loading", *Nucl. Eng. Des.*, **270**, 344-335.
- Priestley, M. (1997), "Displacement-based seismic assessment of reinforced concrete buildings", *J. Earthq. Eng.*, **1**(1), 157-192.
- Saiidi, M. and Sozen, M.A. (1981), "Simple nonlinear seismic analysis of R/C structures", *J. Struct. Div., Proceedings of the American Society of Civil Engineers*, ASCE, **107**(ST5), 937-952.
- Salonikios, T.N., Kappos, A.J., Tegos, I.A. and Penelis, G.G. (1999), "Cyclic load behaviour of low slenderness r/c walls: design basis and test results", *ACI Struct. J.*, **96**(4), 649-660.
- Saritas, A. and Filippou, F.C. (2013), "Analysis of rc walls with a mixed formulation frame finite element", *Comput. Concrete*, **12**(4), 519-536.
- Takeda, T., Sozen, M.A. and Nielsen, N.M. (1970), "Reinforced concrete response to simulated earthquakes", *J. Struct. Div.*, ASCE, **96**(ST12), 2557-2573.
- Thomson, E.D., Perdomo, M.E., Picón, R., Maranteb, M.E. and Flórez-López, J. (2009), "Simplified model for damage in squat RC shear walls", *Eng. Struct.*, **31**, 2215-2223.
- Vecchio, F.J. and Collins, M.P. (1986), "Modified compression-field theory for reinforced concrete beams subjected to shear", *ACI J.*, **83**(2), 219-231.
- Vecchio, F.J., Collins, M.P. and Aspiotis, J. (1994), "High strength concrete elements subjected to shear", *ACI J.*, **91**(4), 423-433.
- Vulcano, A., Bertero, V.V. and Colotti, V. (1988), "Analytical modelling of RC structural walls", *Proceedings, 9th World Conference on Earthquake Engineering*, **6**, Tokyo-Kyoto, Japan, 41-46.
- Wallace, J.W., Elwood, K.J. and Massone, L.M. (2008), "Investigation of the axial load capacity for lightly reinforced wall piers", *J. Struct. Eng.*, ASCE, **134**(9), 1548-1557
- Yu, H. and Hwang, S. (2005), "Evaluation of softened truss model for strength prediction of reinforced concrete squat walls", *J. Eng. Mech.*, ASCE, **131**(8), 839-846.